

溶剂热一锅法合成 Ag-TiO₂ 微球及其对过氧化氢的电化学检测

褚有群 黄章烤 王鑫杭 周梦蕾 赵峰鸣*

(浙江工业大学化学工程学院, 绿色化学合成技术国家重点实验室培训基地, 杭州 310032)

摘要: 采用溶剂热法, 通过调控钛酸四丁酯在醇水浴中的醇解作用和维生素 C 的烯醇还原性制备了细分散的纳米银修饰 TiO₂ 微球。一锅法的制备过程绿色、程序简单, 可获得分布均匀的微球, 直径约 250 nm, 微球表面细分散的银晶格具有(111)晶面特征。构建的 Ag-TiO₂ 微球电极对 H₂O₂ 具有良好的电催化活性, 展现出良好的电化学检测性能, 当 H₂O₂ 的线性范围为 0.1~102 μmol·L⁻¹ 时, 传感电极的灵敏度为 3.13×10⁻³ μA·L·μmol⁻¹·cm⁻², 最低检测限可达 0.04 μmol·L⁻¹。所得传感器具有良好的长期稳定性、重现性和重复性, 一个月后, 性能保持率仍可维持在 82.1%。

关键词: 银; 二氧化钛微球; 过氧化氢; 电化学检测

中图分类号: O646.5 文献标识码: A 文章编号: 1001-4861(2021)07-1258-11

DOI: 10.11862/CJIC.2021.149

One-Pot Solvothermal Synthesis of Ag-TiO₂ Microspheres for Electrochemical Detection of Hydrogen Peroxide

CHU You-Qun HUANG Zhang-Kao WANG Xin-Hang ZHOU Meng-Lei ZHAO Feng-Ming*

(State Key Laboratory Breeding Base of Green Chemistry-Synthesis Technology, College of Chemical Engineering, Zhejiang University of Technology, Hangzhou 310032, China)

Abstract: Herein, finely dispersed silver decorated TiO₂ microspheres have been synthesized by one-pot solvothermal method using tetrabutyl titanate and vitamin C in ethanol. The structure of TiO₂ microsphere and high dispersion of nano silver were regulated by the alcoholysis of tetrabutyl titanate and reducibility of enol in vitamin C. The one-pot method was beneficial to reduce the complex procedures and obtain uniform spherical particles with a diameter of 250 nm. The silver lattice stripes integrated into the surface of microspheres show crystal plane (111) characteristics. The composite electrode exhibited excellent electrocatalytic activity of H₂O₂. The developed sensor allowed the detection of H₂O₂ with the linear range of 0.1~102 μmol·L⁻¹, sensitivity of 3.13×10⁻³ μA·L·μmol⁻¹·cm⁻² and detection limit of 0.04 μmol·L⁻¹. The resulting device also had longterm stability, reproducibility and repeatability. The performance could be maintained at 82.1% after a month.

Keywords: silver; titanium dioxide microsphere; hydrogen peroxide; electrochemical detection

0 Introduction

Hydrogen peroxide has been used frequently as an eco-friendly chemical in industrial production, food preservation and environmental protection^[1-3]. It is of

great significance to develop the method for accurate detection of hydrogen peroxide because H₂O₂ might be an intermediate for industrial processes and a by-product of chemical or biological reaction^[4-8]. Since traditional detecting techniques have shortcomings of

收稿日期: 2020-10-16。收修改稿日期: 2021-05-26。

浙江省自然科学基金(No.LY17B050006)和国家重点研究开发计划(No.2017YFB0307503)资助。

*通信联系人。E-mail: zhaofm@zjut.edu.cn

high cost, time consuming and complex operation, electrochemical detection may be preferable due to its low consumption, fast response and simplicity^[9-12]. Although enzyme-based electrochemical sensors exhibit specific advantages, their application is limited by stability issues and high cost^[13-15]. Therefore, non-enzyme electrochemical sensors have become one of the research hotspots for H₂O₂ detection due to their high stability and no-dependency on temperature, ion concentration, pH and toxic chemicals^[16-19]. In recent years, various noble metal composites have been widely used in non-enzymatic sensor with the development of material preparation technology. Recent researches show that silver is the best conductive metal with good chemical properties^[20], catalytic properties^[21] and biocompatibility^[22]. Hence, it is widely used in the fields of electronics, chemical engineering, biomedicine, medicine, and daily necessities^[23]. Many methods have been used to prepare silver nanoparticles, such as template method^[24-25], wet chemical method^[26-27], electrochemical method^[28-29] and polyol method^[30]. However, the catalytic properties are often affected due to their tendency to agglomerate during preparation. Particle's agglomera-

tion is a key problem not to be ignored for the preparation of nano silver.

In order to prepare highly dispersed nano silver, in this paper titanium dioxide (TiO₂) was introduced as carrier due to its excellent optical properties^[31], electrical properties^[32] and certain catalytic activity^[33]. The preparation method of titanium dioxide is simple and its morphology is highly controllable^[34-36]. It has attracted the more attention for electrochemical sensing and is often used as catalyst carrier^[37-38]. In this work, silver decorated TiO₂ microspheres (Ag-TiO₂ MS) were synthesized by one-pot solvothermal method. As shown in Fig. 1, an alcoholysis of tetrabutyl titanate (TBOT) was controlled in alcohol solvent to obtain TiO₂ microsphere and a reducing reaction of enol in vitamin C (VC) was performed with surrounding nano silver uniform dispersion during the high temperature and pressure. As a result, the one-pot reaction can still retain the metallic properties of silver. Herein, Ag-TiO₂ composite was provided for detecting H₂O₂. Combining this composite with other catalytic materials can promote new ideas for electrochemical sensors.

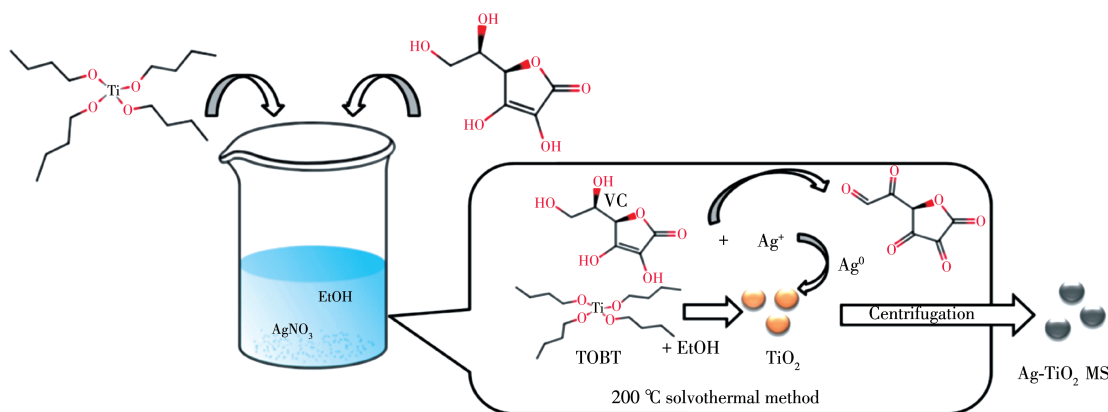


Fig.1 Schematic illustration of one-pot solvothermal synthesis of finely-dispersed Ag-TiO₂ MS

1 Experimental

1.1 Materials and reagents

The reagents required in synthesis of Ag-TiO₂ MS were silver nitrate (AgNO₃, 99.8%), VC (99.7%) and TBOT (99.0%) purchased from Aladdin, China. The reagents used for electrochemical measurements included hydrogen peroxide (H₂O₂, 30%), urea

(99.0%), glucose (*L*-Glu, 98%) and lactose (Lac, 98%) that were purchased from Aladdin, China. Phosphate buffer solution (PBS, pH=7.0, 0.02 mol·L⁻¹) as supporting electrolyte was prepared with KH₂PO₄ and KOH (Sinopharm, China).

1.2 One-pot synthesis of Ag-TiO₂ MS

In a typical procedure, 30 mmol·L⁻¹ VC and 0.03 g AgNO₃ were dissolved in 70 mL absolute ethanol in a

beaker with magnetic stirring, and then $8 \text{ mmol}\cdot\text{L}^{-1}$ TBOT was added to form a transparent solution with brown color. Subsequently, the solution was transferred into 100 mL Teflon-line stainless steel autoclave (Microreactor, Yanzheng Instrument Ltd., Shanghai) and heated in an oven at $200 \text{ }^\circ\text{C}$ for 7 h. After the autoclave was cooled down to room temperature in air, the solid product (Ag-TiO₂ MS) was separated by centrifugation, washed with deionized water and absolute alcohol several times, and dried in vacuum at $60 \text{ }^\circ\text{C}$ for 6 h. TiO₂ microspheres (TiO₂ MS) can be synthesized by the same method just without adding AgNO₃.

1.3 Preparation and characterization of Ag-TiO₂ MS electrode

Prior to use, glassy carbon electrode (GCE, $\phi=3.0 \text{ mm}$, $S=0.0707 \text{ cm}^2$) was polished with 300 and 50 nm aluminum oxide powders to a mirror-like, respectively, and then washed successively with acetone, ethanol and double-distilled water for several times. A homogeneous mixture was formed by adding 2.0 mg Ag-TiO₂ MS into 100 μL double-distilled water, 100 μL absolute ethanol and 10 μL Nafion (5%, *w/w*). The mixture was sonicated for 30 min. The preparation procedures of Ag-TiO₂ MS electrode as follows: 3.5 μL mixture was dropped on the surface of GCE and dried in ambient air for 20 min.

The morphology was examined by high resolution transmission electron microscopy (HR-TEM, 300 kV), high angle annular dark field scanning transmission electron microscopy (HAADF-STEM, 300 kV), coupled with energy dispersive X-ray spectrometer (EDX), using Cu *K* α radiation and spherical-aberration corrected field-emission transmission electron microscope

(Philips-FEI, Tecnai G2 F30 S-Twin). The oxidation states of chemical species were detected by X-ray photoelectron spectroscopy (XPS, Kratos Axis Ultra DLD) using a focused monochromatized Al *K* α operated at 300 W. The binding energies were referenced to the C1s line at 284.6 eV from adventitious carbon.

1.4 Electrochemical measurement of H₂O₂

Electrochemical measurements were performed on an Ivium potentiostat in N₂-saturated $0.02 \text{ mol}\cdot\text{L}^{-1}$ PBS (pH 7.0), with or without H₂O₂, using a three-electrode cell with the Ag-TiO₂ MS electrode as working electrode, a Pt foil counter electrode, and a Ag/AgCl reference electrode. The electrochemical impedance spectroscopy (EIS) was measured by applying amplitude of 5.0 mV over the frequency ranging from 10^5 to 10^{-2} Hz. For electrochemically sensing H₂O₂, the sensitivity, stability, reproducibility and anti-interfering activity studies were also performed in N₂-saturated $0.02 \text{ mol}\cdot\text{L}^{-1}$ PBS (3.0 mL, pH 7.0) using chronoamperometry at -0.3 V .

2 Results and discussion

2.1 Characterization of Ag-TiO₂ MS

Fig.2 shows a typical SEM image of the TiO₂ MS and Ag-TiO₂ MS. As shown in Fig.2a, the average size of TiO₂ MS was hundred nanometers but not uniform. The inset of Fig.2a showed a rough TiO₂ MS with a diameter of about 250 nm. As shown in Fig.2b, the layers of material superimposed on the surface of Ag-TiO₂ MS and the surface roughness of the spheres was improved by Ag modification. The average diameter of each sphere was about 200~300 nm. In addition, it can be found that some spheres twined together, which may

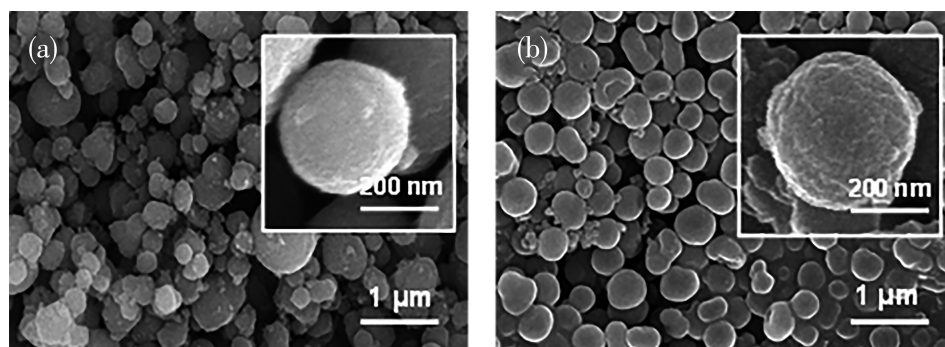


Fig.2 SEM images of TiO₂ MS (a) and Ag-TiO₂ MS (b)

be related to the growth process of Ag-TiO₂ MS. By changing the reaction time, we found that the adhesion phenomenon was gradually obvious with the increase of solvent heat time during the growth of TiO₂ MS (Fig.S1).

XPS spectra was further used to confirm the surface chemical composition and oxidation state. Fig. 3 shows the high resolution XPS spectra of Ti2p, O1s, Ag3d and Ag MVV for Ag-TiO₂ MS. Ti2p spectra can be divided into Ti2p_{1/2} and Ti2p_{3/2} peaks, and the peaks at 463.7 and 457.9 eV can be assigned to Ti—O bonds. The O1s XPS spectrum for Ag-TiO₂ MS at 530.2 eV is ascribed to Ti—O bonds. The Ag3d XPS spectrum of Ag-TiO₂ MS shows peaks at 368.0 and 374.0 eV, corresponding to the Ag3d_{5/2} and Ag3d_{3/2}, respectively. The Auger parameter (α'), which is defined as the sum of the kinetic energy of the Auger electron (α_{AgM_4VV}) and the binding energy of the core level Ag3d_{5/2} ($\alpha_{Ag3d_{5/2}}$), can be calculated by the equation of $\alpha' = \alpha_{AgM_4VV} + \alpha_{Ag3d_{5/2}}$ ^[39]. The characteristic peak appeared in

the Ag M_{4VV} XPS spectrum at 358.0 eV and the α' was calculated to be 726.0 eV, which is ascribed to Ag⁰ in Ag-TiO₂ MS.

XRD patterns of TiO₂ MS and Ag-TiO₂ MS are shown in Fig.4. It can be seen that TiO₂ MS might be amorphous and this can be confirmed by the selected area electron diffraction (SAED, Fig.S2). Four diffraction peaks with 2 θ values of 38.1°, 44.3°, 64.4° and 77.4° can be assigned to (111), (200), (220) and (311) planes of face-centered cubic (fcc) Ag.

Fig.5a and 5d show the TEM images of TiO₂ MS and Ag-TiO₂ MS, which reveal the detailed structure of the spherical morphology. Both in TiO₂ MS and Ag-TiO₂ MS, there was no obvious lattice stripe of TiO₂, which indicates that it mainly exists in amorphous form. However, Ag⁰ were grown on the surface of Ag-TiO₂ MS. These Ag nanoparticles (Ag NPs) had highly crystalline and the lattice spacing was determined to be 0.236 nm, which is attributed to (111)

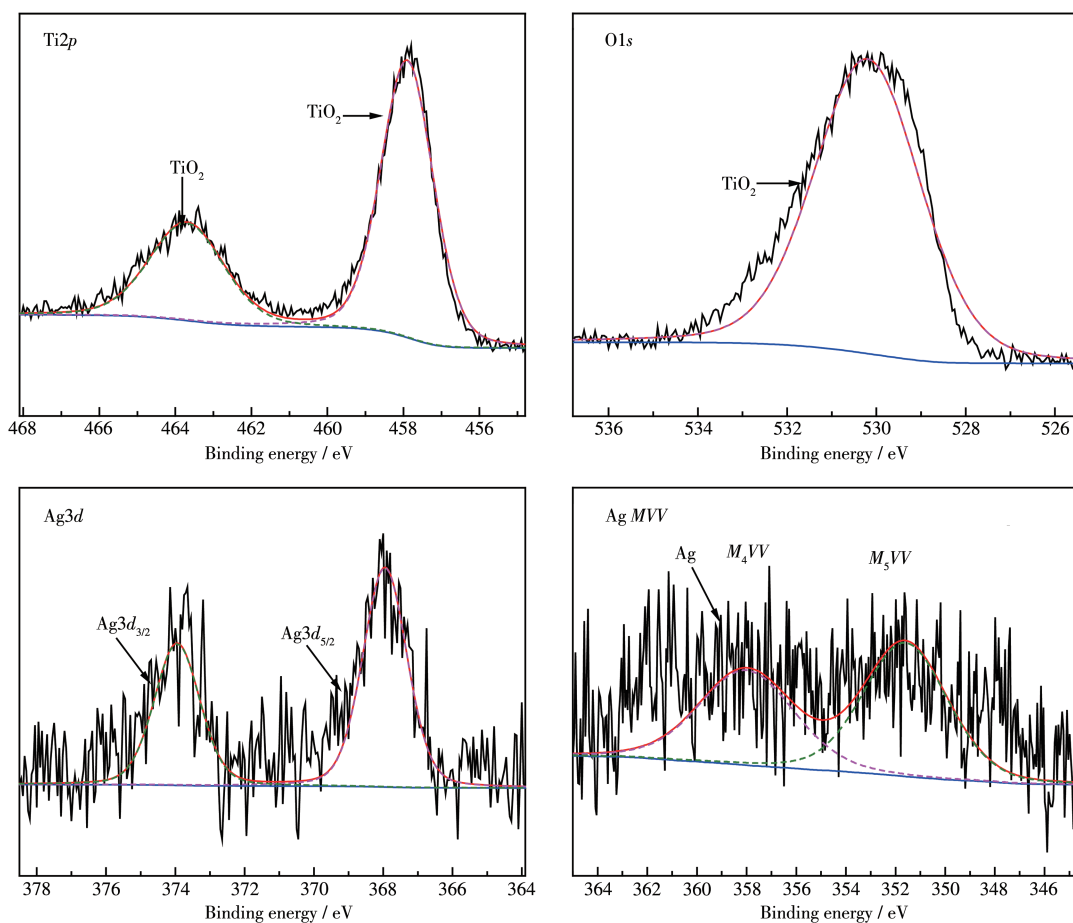


Fig.3 XPS spectra of Ag-TiO₂ MS

plane of Ag (Fig.5f).

Furthermore, the composition of TiO₂ MS and Ag-TiO₂ MS was confirmed by EDX. Fig.6 illustrated that the TiO₂ MS included Ti, O elements and the Ag-TiO₂ MS included Ti, O, and Ag elements, suggesting that TiO₂ MS and Ag-TiO₂ MS were successful by one-pot synthesis method. In addition, Fig.7 is the HAADF-STEM images and the corresponding EDX mappings of TiO₂ MS and Ag-TiO₂ MS. Obviously, it proved that the distribution of Ti, O and Ag elements was relatively homogenous, and Ag⁰ was highly dispersed on the surface of TiO₂ MS.

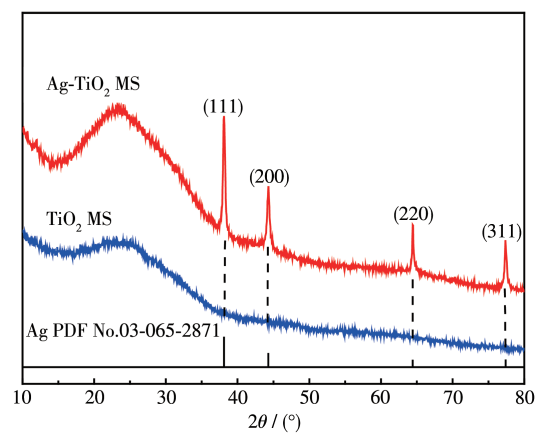
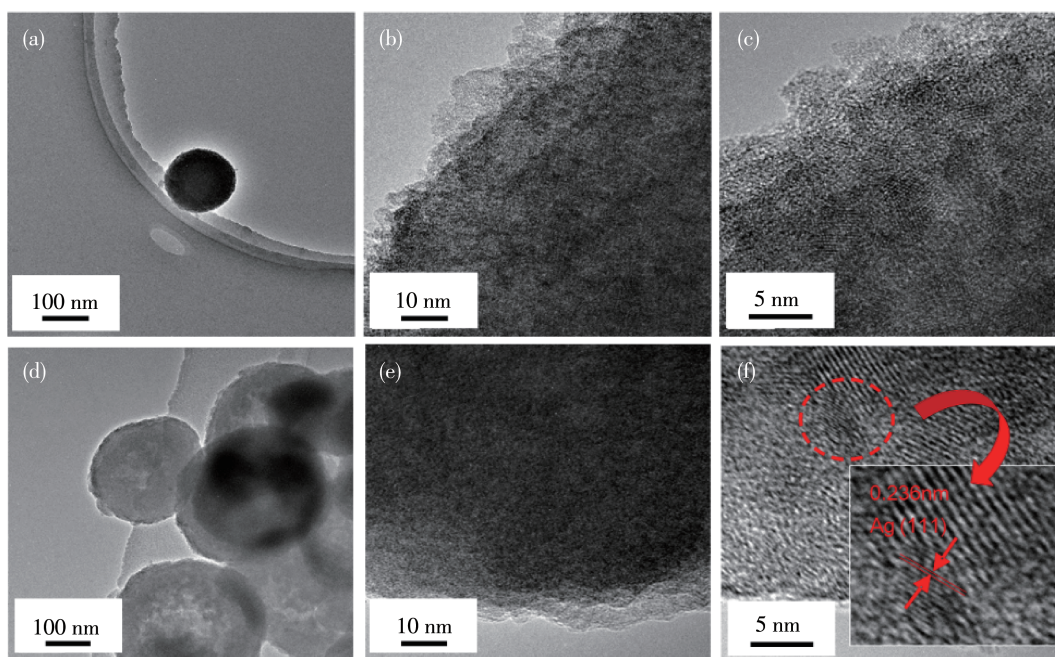


Fig.4 XRD patterns of TiO₂ MS and Ag-TiO₂ MS



Inset shows the magnified image with clear lattice fringes

Fig.5 TEM images of TiO₂ MS (a~c) and Ag-TiO₂ MS (d~f)

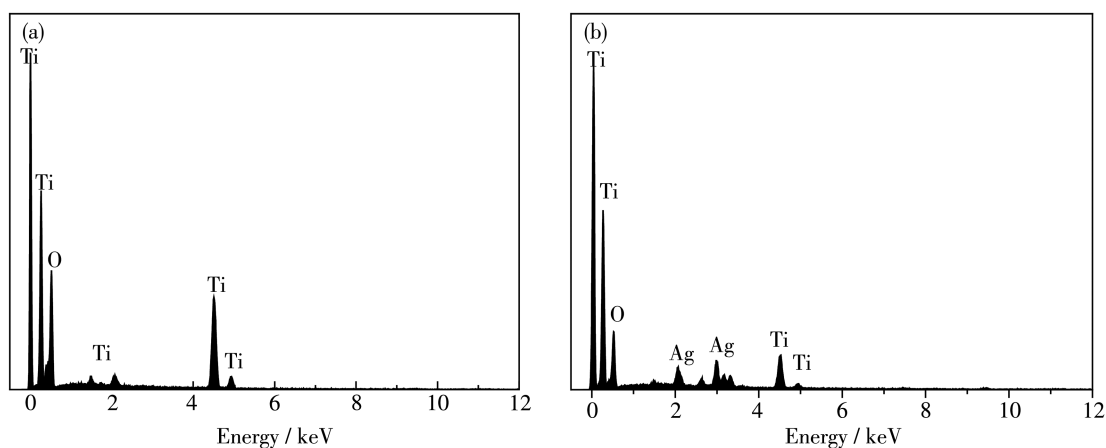


Fig.6 EDX spectra of (a) TiO₂ MS and (b) Ag-TiO₂ MS

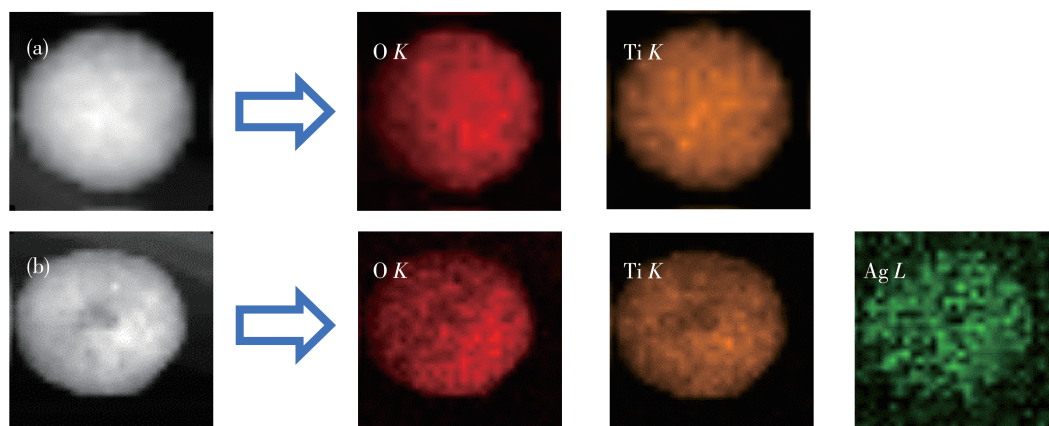


Fig.7 HAADF-STEM images and the corresponding EDX mappings of (a) TiO₂ MS and (b) Ag-TiO₂ MS

2.2 Electrochemical performance of Ag-TiO₂ MS for H₂O₂

Cyclic voltammetry (CV) was employed to characterize the electrochemical behavior of the electrode. Fig.8 shows the CV curves of TiO₂ MS and Ag-TiO₂ MS electrodes in 0.02 mol·L⁻¹ PBS (pH 7.0) with and without 1 000 μmol·L⁻¹ H₂O₂ at scan rates of 20 mV·s⁻¹. Compared with TiO₂ MS, Ag-TiO₂ MS electrode showed a reduction peak at around -0.4 V, suggesting the strong reduction ability of Ag-TiO₂ MS for H₂O₂.

The electrochemical performance of Ag-TiO₂ MS electrode towards H₂O₂ reduction was further examined via changing the H₂O₂ concentrations (Fig.9) and scan rates (Fig.10). As seen in Fig.9b, the increase of H₂O₂ concentration led to a regular increase in the reduction peak current in Ag-TiO₂ MS electrodes. Compared with Fig.9a, it was no obvious response to hydrogen peroxide for TiO₂ MS electrode, indicating that the Ag-TiO₂ MS electrodes have good electrocatalytic activity and

an application prospect as a sensor after loading with Ag.

The kinetic parameters were further calculated by the relation graph of H₂O₂ concentration and scan rates (Fig.10). In the irreversible process, the diffusion coefficient (*D*₀) and reaction rate constant (*k*₀) were calculated.

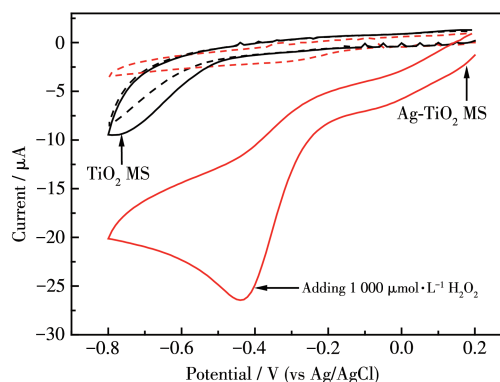


Fig.8 CVs of TiO₂ MS (black curves) and Ag-TiO₂ MS (red curves) electrodes in 0.02 mol·L⁻¹ PBS (pH 7.0) with (solid curves) or without (dotted curves) 1 000 μmol·L⁻¹ H₂O₂ at 20 mV·s⁻¹

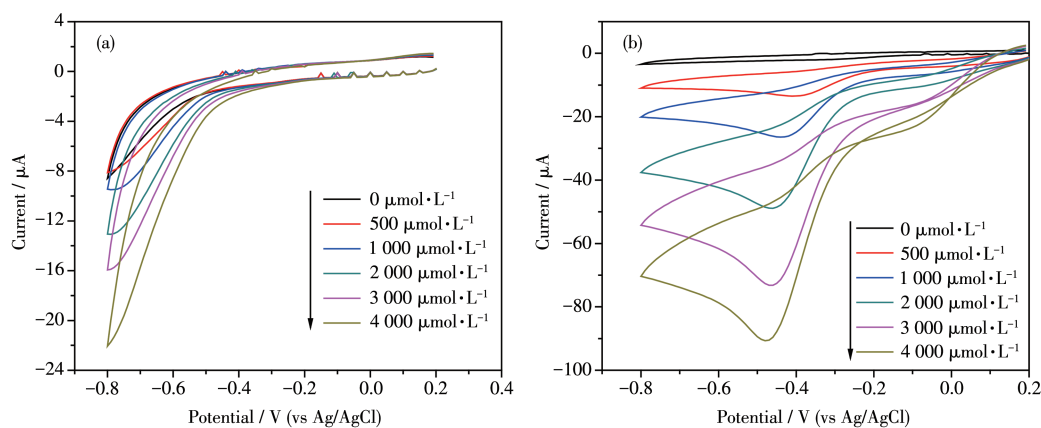


Fig.9 CVs of TiO₂/MS (a) and Ag-TiO₂/MS (b) electrodes at 20 mV·s⁻¹ with adding different concentrations of H₂O₂

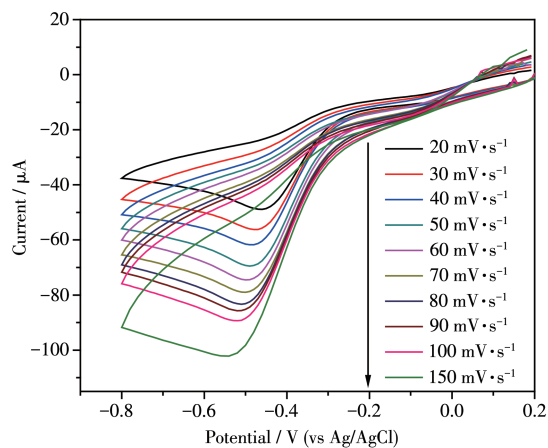


Fig.10 CVs of Ag-TiO₂ MS electrode in the presence of 2 000 μmol·L⁻¹ H₂O₂ at different the scan rates

ed using the Eq.1 and Eq.2^[40].

$$I_p = 2.99 \times 10^5 n^{3/2} \alpha^{1/2} A c_0 D_0^{1/2} v^{1/2} \quad (1)$$

$$I_p = 0.227 n F A c_0 k_0 \exp[-\alpha F (E_p - E_{1/2}) / (RT)] \quad (2)$$

Where I_p is the peak current (A), n is the number of electrons, F is Faraday constant, A is the area of the electrode (cm²), c_0 is the concentration of H₂O₂ (mol·L⁻¹), E_p is the peak potential (V), $E_{1/2}$ is the half-wave peak potential (V), α is the charge transfer coefficient, v is the scan rate (V·s⁻¹). The concentration of H₂O₂ was 2 000 μmol·L⁻¹ and the electroactive surface area for Ag-TiO₂ MS was 0.070 7 cm². Eq.3 is built by evaluating the logarithm of Eq.2.

$$\ln I_p = -\alpha F (E_p - E_{1/2}) / (RT) + \ln(0.227 n F A c_0 k_0) \quad (3)$$

The linear relationship of I_p and $v^{1/2}$ for Ag-TiO₂ MS electrode was $I_p = 120.07 v^{1/2} + 4.992$ ($R^2 = 0.996$) (Fig.11a). The calculated D_0 value on Ag-TiO₂ MS electrode was 1.96×10^{-5} cm²·s⁻¹.

The relationship of $\ln I_p$ and $(E_p - E_{1/2})$ for Ag-TiO₂

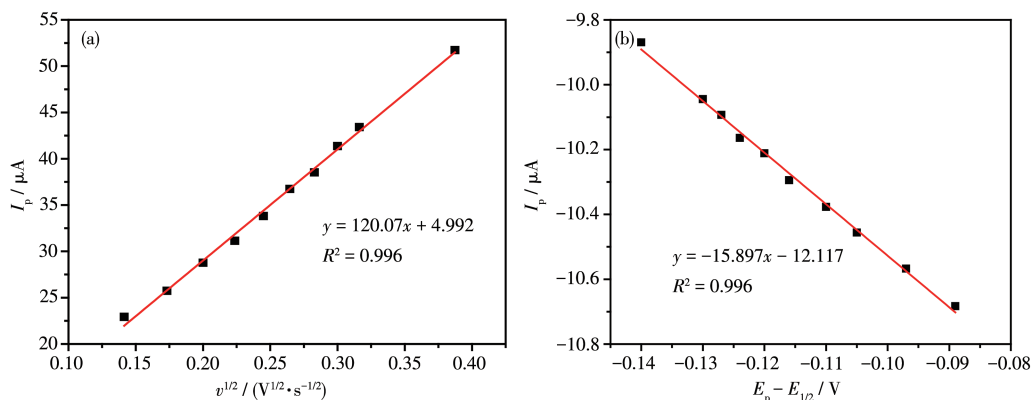
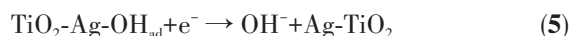
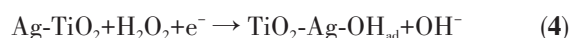


Fig.11 (a) Relationship of I_p and $v^{1/2}$ and (b) relationship of $\ln I_p$ and $(E_p - E_{1/2})$ for Ag-TiO₂ MS electrode

MS was $\ln I_p = -15.897(E_p - E_{1/2}) - 12.117$ ($R^2 = 0.996$). The calculated k_0 value on Ag-TiO₂ MS electrode was 1.45×10^{-3} cm²·s⁻¹.

In order to illustrate the effect of the loaded silver, EIS of TiO₂ MS and Ag-TiO₂ MS electrodes were carried out. The obtained Nyquist plots are shown in Fig.12 and the constant phase angle element (CPE) replaces the electrode double layer capacitance in the equivalent circuit diagram. Two typical semicircles can be observed at high frequency range and the low frequency region, respectively. Based on the equivalent circuit, charge-transfer resistance (R_{ct}) can be determined from the diameter of the left most semicircle, and the polarization resistance (R_p) can be determined from the diameter of the second semicircle. The parameters obtained from the fitting curves of EIS are shown in Table 1. The ohmic serial resistance (R_s) can be obtained by the intercept on the real axis at high frequency. The R_{ct} of TiO₂ MS and Ag-TiO₂ MS electrodes were 726 and 613 Ω, and the R_p were 291.5 and 28.34 kΩ, respectively. Obviously, the R_{ct} and R_p of Ag-TiO₂ MS were lower than that of TiO₂ MS, which conformed that Ag-TiO₂ MS has better electronic conductivity and electrochemical reaction rate.

In conclusion, hydrogen peroxide can be adsorbed by nano silver in neutral medium^[41], the cathodic reaction process may be shown as follows:



Successful loading of nano silver will make the reaction step 4 and 5 easier to perform, which provide

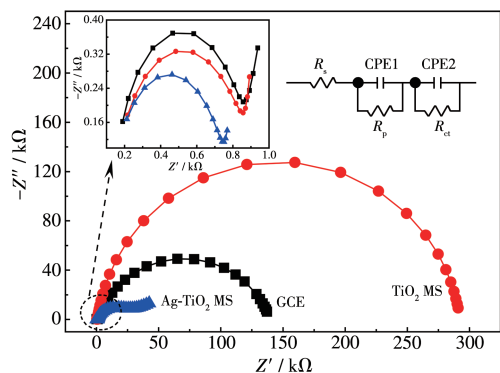


Fig.12 Nyquist plots of Ag-TiO₂ MS, TiO₂ MS and GCE electrodes

Table 1 Parameters obtained from the fitting curves of EIS in Fig.12

Sample	R_s / Ω	R_{ct} / Ω	$R_p / k\Omega$
Ag-TiO ₂ MS	126.9	613	28.34
TiO ₂ MS	133.9	726	291.5
GCE	135.4	675	138.9

higher electrochemical reaction rates for catalytic reactions and effectively improve the electrical conductivity of the material.

2.3 Detection performance of Ag-TiO₂ MS towards H₂O₂

Amperometric response ($I-t$, the relation between current and time) curves were performed with the successive addition H₂O₂ into a stirring electrochemical cell containing 3 mL PBS (0.02 mol·L⁻¹, pH 7.0) at an optimized potential of -0.3 V (Fig.13). For Ag-TiO₂ MS electrode, each response current step showed a downward trend between 0.1 to 102 μmol·L⁻¹ and an upward trend between 478 to 699 μmol·L⁻¹. It is clear

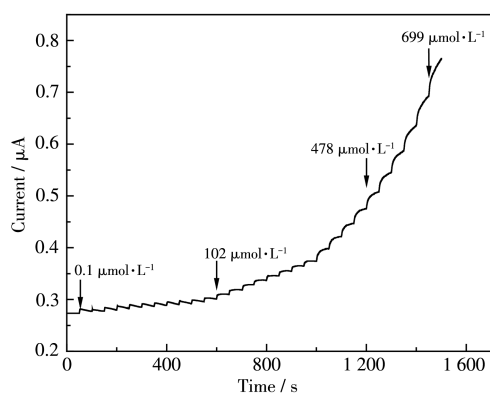


Fig.13 $I-t$ curve of Ag-TiO₂ MS in 0.02 mol·L⁻¹ PBS (pH 7.0) with the successive adding H₂O₂

that the response current can remain stable only in the intermediate concentration range.

Fig. 14 presents the linear fitting relationships between the current response and H₂O₂ concentration. The current responses as functions of H₂O₂ concentration can be represented by three different linear equations, which are valid at different concentration ranges. The linear regression equations of Ag-TiO₂ MS were $I=2.21 \times 10^{-4} c_{\text{H}_2\text{O}_2} + 0.278$ ($R^2=0.979$) for $c_{\text{H}_2\text{O}_2}=0.1 \sim 102$ μmol·L⁻¹, $I=5.41 \times 10^{-4} c_{\text{H}_2\text{O}_2} + 0.240$ ($R^2=0.997$) for $c_{\text{H}_2\text{O}_2}=102 \sim 478$ μmol·L⁻¹ and $I=1.234 \times 10^{-3} c_{\text{H}_2\text{O}_2} - 0.109$ ($R^2=0.985$) for $c_{\text{H}_2\text{O}_2}=478 \sim 699$ μmol·L⁻¹. The limit of detection (LOD) was determined by using the equation $\text{LOD}=3S_B/b$, where b is the slope of the calibration curve and S_B is the standard deviation of the blank solution. The LOD ($S/N=3$) of Ag-TiO₂ MS sensor was calculated to be 0.04 μmol·L⁻¹. Meanwhile the obtained sensitivity of Ag-TiO₂ MS was 3.13×10^{-3} μA·L·μmol⁻¹·cm⁻².

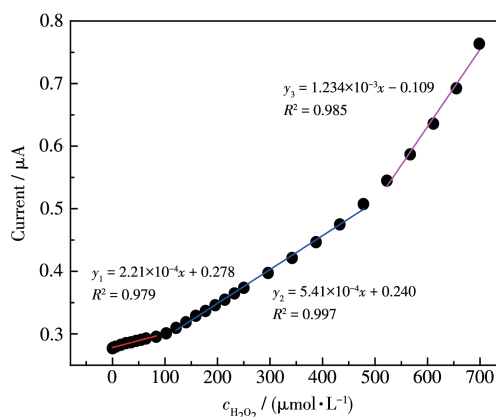


Fig.14 $I-c_{\text{H}_2\text{O}_2}$ linear fitting results for Ag-TiO₂ MS

Compared with several previous reports, as shown in Table 2, the as-prepared sensors exhibited the lowest detection limit with good linear range and the fast-current response towards H₂O₂, which it can be attributed to the special properties of Ag-TiO₂ MS. In the composite, the metallic oxide plays a significant as substrate material. Therefore, the good electron transfer efficiency of the Ag-TiO₂ MS may lead to the short response time.

2.4 Selectivity, reproducibility, repeatability and storage stability of Ag-TiO₂ MS electrodes

Fig.15a is the long-term stability chart of Ag-TiO₂

Table 2 Comparison of H_2O_2 sensors reported previously with Ag-TiO₂ MS sensor

Sensor	$c_{\text{H}_2\text{O}_2} / (\mu\text{mol}\cdot\text{L}^{-1})$		Reference
	Linear range	Detection limit	
Prussian blue-TiO ₂	1.5~90	1.5	[42]
Thionin/DNA/nano-TiO ₂	50~22 300	50	[43]
TiN	20~3 000	250	[44]
AgNPs-TiO ₂ nanowires	100~60 000	1.7	[45]
Cu ₂ O/TiO ₂ /sepiolite electrode	20~2 360	1.7	[46]
Cu ₂ O/TiO ₂ nanotubes array	500~80 00	90.5	[47]
Pd _{0.7} Au _{0.3} /carbon nanotube	1~19 000	0.3	[48]
Fe ₃ O ₄ /graphene oxide/pristine graphene	0.5~277	0.09	[49]
Au@Ag nanorods	0~100	3.2	[50]
Au-Ag/Co ₃ O ₄ nanofibers	0.05~5 000	0.01	[51]
CuCo ₂ O ₄ hollow microspheres	10~8 900	0.75	[52]
Graphene nanosheets@FeOOH	0.25~1 200	0.08	[53]
AuNPs-NH ₂ /Cu-metal-organic framework	5~850	1.2	[54]
Co ₃ N nanowire/Ti mesh	0.1~2 500	0.05	[55]
Ag/Sn ₃ O ₄ /GCE	0.8~52 000	0.8	[56]
Pt/C-CeO ₂	10~30 000	2	[57]
BiVO ₄ /TiO ₂	5~200	5	[58]
Ag-TiO ₂ MS	0.1~102	0.04	This work

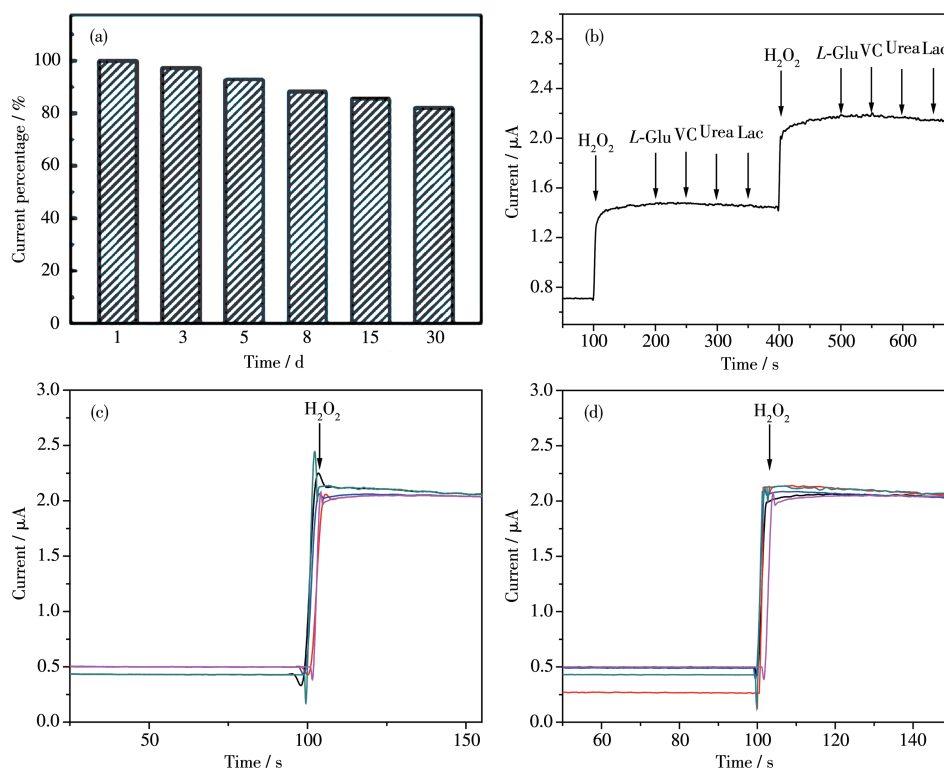


Fig.15 (a) Normalized response of Ag-TiO₂ MS toward $100 \mu\text{mol}\cdot\text{L}^{-1} \text{H}_2\text{O}_2$ in PBS (pH 7.0) at -0.3 V in 30 days; (b) $I-t$ curve of Ag-TiO₂ MS in $0.02 \text{ mol}\cdot\text{L}^{-1}$ PBS (pH 7.0) for selective studies with adding $500 \mu\text{mol}\cdot\text{L}^{-1} \text{H}_2\text{O}_2$, L-Glu, VC, urea and Lac; (c) Reproducibility studies with adding $500 \mu\text{mol}\cdot\text{L}^{-1} \text{H}_2\text{O}_2$; (d) Repeatability studies with adding $500 \mu\text{mol}\cdot\text{L}^{-1} \text{H}_2\text{O}_2$

MS electrode. The electrodes were stored at room temperature and exposed to air before use. After one month, the current response of the sensor to H₂O₂ decreased by 17.9%. By analysis of SEM, XRD, TEM and XPS (Fig. S3, S4, S5, S6), it can be seen that the catalytic performance of the Ag-TiO₂ MS electrode was decreased due to the weakening of crystalline surface strength and the destruction of the morphological structure. Fig. 15b is the *I-t* curve of Ag-TiO₂ MS in 0.02 mol·L⁻¹ PBS (pH 7.0) for selective studies. 500 μmol·L⁻¹ H₂O₂, L-Glu, VC, urea and Lac were added successively. The results showed that the addition of H₂O₂ caused a significant current response, and further addition of interfering substances did not have an obvious reaction, indicating that Ag-TiO₂ MS has good selectivity and sensitivity for H₂O₂.

Ag-TiO₂ MS electrodes were prepared in parallel to evaluate the electrocatalytic activity sensor reproducibility for H₂O₂. After calculation, 5 electrodes were subsequently prepared under the same conditions, and the relative standard deviation of current response was only 2.0% (Fig. 15c). The same electrode was repeatedly measured for 5 times, and the relative standard deviation of response was 3.7% (Fig. 15d).

3 Conclusions

In summary, Ag-TiO₂ MS were successfully synthesized by one-pot method. Serving as a H₂O₂ detection electrode, Ag-TiO₂ MS presents excellent nonenzymatic H₂O₂ sensing performance in terms of wide linear range and reliable stability. It is believed that the Ag-TiO₂ MS presents broad applications in the development of nonenzymatic H₂O₂ electrochemical sensors and the immobilization of finely dispersed silver on TiO₂ microsphere paves an effective way to construct H₂O₂ detection electrode. The Ag-TiO₂ MS material can be further modified in subsequent research, such as high-temperature renitriding into titanium nitride to enhance its stability for better application in electrochemical sensors.

Supporting information is available at <http://www.wjhxxb.cn>

Acknowledgements: This work was supported by the

Natural Science Foundation of Zhejiang Province, China (Grant No. LY17B050006) and the National Key Research and Development Plan (Grant No. 2017YFB0307503).

References:

- [1] Chen W, Cai S, Ren Q Q, Wen W, Zhao Y D. *Analyst*, **2012**, **137**:49-58
- [2] Rodrigo A B S, Rodrigo H O M, Eduardo M R, Rodrigo A A M. *Food Chem.*, **2012**, **133**(1):200-204
- [3] Sekar N K, Gumpu M B, Ramachandra B L, Nesakumar N, Sankar P, Babu K J, Krishnan U M, Rayappan J B B. *J. Nanosci. Nanotechnol.*, **2018**, **18**(6):4371-4379
- [4] Wu T T, Englehardt J D. *Environ. Sci. Technol.*, **2012**, **46**(4):2291-2298
- [5] Anastasia S I, Anna D M, Sergey V A, Konstantin A S. *Food Chem.*, **2019**, **283**:431-436
- [6] Li J M, Shah A M. *J. Am. Soc. Nephrol.*, **2003**, **14**:221-226
- [7] Huang B K, Sikes H D. *Redox Biol.*, **2014**, **2**:955-962
- [8] Li M, Gao H F, Wang X F, Wang Y F, Qi H L, Zhang C X. *Microchim. Acta*, **2017**, **184**(2):603-610
- [9] Nitinaivinij K, Parnklang T, Thammacharoen C, Ekgasit S, Wongravee K. *Anal. Methods*, **2014**, **6**(24):9816-9824
- [10] Gimeno P, Bousquet C, Lassu N, Maggio A F, Lempereur L. *J. Pharm. Biomed. Anal.*, **2015**, **107**:386-393
- [11] Kawde A N, Aziz M, Baig N, Temerk Y. *J. Electroanal. Chem.*, **2015**, **740**:68-74
- [12] Ensafi A A, Abarghoui M M, Rezaei B. *Sens. Actuators B*, **2014**, **196**:398-405
- [13] Updike S J, Hicks G P. *Nature*, **1967**, **214**(5092):986
- [14] Santos A, Macías G, Ferré-Borrull J, Pallares J, Marsal L F. *ACS Appl. Mater. Interfaces*, **2012**, **4**(7):3584-3588
- [15] Amor-Gutiérrez O, Rama E C, Costa-García A, Fernandez-Abedul M T. *Biosens. Bioelectron.*, **2017**, **93**:40-45
- [16] 吕雪义, 刘俊果, 朱艳艳. *无机化学学报*, **2020**, **36**(9):1675-1682
LÜ X Y, LIU J G, ZHU Y Y. *Chinese J. Inorg. Chem.*, **2020**, **36**(9):1675-1682
- [17] Zaibudeen A W, Philip J. *Sens. Actuators B*, **2018**, **255**:720-728
- [18] Liu F Y, Peng W, Zhang Q Q, Wang Z Y, Liu Y Y, Zheng Z K, Qin X Y, Zhang X Y, Dai Y, Li L, Huang B B. *Anal. Bioanal. Chem.*, **2018**, **410**:7663-7670
- [19] Baghayeri M, Alinezhad H, Tarahomi M, Fayazi M, Ghanei-Motlagh M, Maleki B. *Appl. Surf. Sci.*, **2019**, **478**:87-93
- [20] Gholami M, Koivisto B. *Appl. Surf. Sci.*, **2019**, **467**:112-118
- [21] 褚有群, 王玲巧, 黄章烤, 徐颖华, 赵峰鸣. *无机化学学报*, **2020**, **36**(3):555-556
CHU Y Q, WANG L Q, HUANG Z K, XU Y H, ZHAO F M. *Chinese J. Inorg. Chem.*, **2020**, **36**(3):555-556
- [22] Qin X Y, Lu W B, Luo Y L, Lu W B, Chang G H, Asiri A M, Al-Youbi A O, Sun X P. *Electrochim. Acta*, **2012**, **74**:275-279

- [23] Alrub A M. *Surf. Sci.*, **2019**, **681**:70-75
- [24] Li C H, Jamison A C, Rittikulsittichai S, Lee T C, Lee T R. *ACS Appl. Mater. Interfaces*, **2014**, **6**:19943-19950
- [25] Wang L, Yang W T, Zhu W, Guan X G, Xie Z G, Sun Z M. *Inorg. Chem.*, **2014**, **53**:11584-11588
- [26] Zhai A X, Cai X H, Du B. *Trans. Nonferrous Met. Soc. China*, **2014**, **24**(5):1452-1457
- [27] Singh J, Tripathi N, Mohapatra S. *Nano-Struct. Nano-Objects*, **2019**, **18**:92-99
- [28] Li B E, Hao J Z, Min Y, Xin S G, Guo L T, He F, Liang C Y, Wang H S, Li H P. *Mater. Sci. Eng. C*, **2015**, **51**:80-86
- [29] Sahyar B Y, Kaplan M, Ozsoz M, Celik E, Otles S. *Bioelectrochemistry*, **2019**, **130**:107327
- [30] Li W, He Y, Xu J, Wang W Y, Zhu Z T, Liu H. *J. Alloys Compd.*, **2019**, **803**:332-340
- [31] Xia L, Yang Y, Cao Y, Liu B, Li X X, Chen X Y, Song H, Zhang X M, Gao B, Fu J J. *Surf. Coat. Technol.*, **2019**, **365**:237-241
- [32] Zheng L X, Dong Y C, Bian H D, Lee C, Lu J, Li Y Y. *Electrochim. Acta*, **2016**, **203**:257-264
- [33] Arunachalam M, Yun G, Ahn K S, Seo W S, Jung D S, Kang S H. *Int. J. Hydrogen Energy*, **2018**, **43**(34):16458-16467
- [34] Zhao F M, Yan F, Qian Y, Chu Y Q, Ma C A. *Int. J. Electrochem. Sci.*, **2012**, **7**(12):12931-12940
- [35] Chang B Y S, Huang N M, An'amt M N, Marlinda A R, Norazriena Y, Muhamad M R, Harrison I, Lim H N, Chia C H. *Int. J. Nanomed.*, **2012**, **7**:3379-3387
- [36] Ding S J, Huang F Q, Mou X L, Wu J J, Lu X J. *J. Mater. Chem.*, **2011**, **21**(13):4888-4892
- [37] Wang S L, Qian H H, Hu Y, Dai W, Zhong Y J, Chen J F, Hu X. *Dalton Trans.*, **2013**, **42**(4):1122-1128
- [38] Zhao S D, Chen J R, Liu Y F, Jiang Y, Jiang C G, Yin Z L, Xiao Y G, Cao S S. *Chem. Eng. J.*, **2019**, **367**:249-259
- [39] Zhao F M, Zhou M L, Wang L Q. *J. Electroanal. Chem.*, **2019**, **833**:205-212
- [40] Bard A J, Faulkner L R. *Electrochemical Methods Fundamentals and Applications*. New York: John Wiley & Sons Inc, **2001**.
- [41] Lim S P, Shahid M M, Rameshkumar P, Huang N M, Che L M. *J. Mater. Sci.-Mater. Electron.*, **2020**, **31**(8):6017-6026
- [42] Chu Z Y, Shi L, Liu Y, Jin W Q, Xu N P. *Biosens. Bioelectron.*, **2013**, **47**:329-334
- [43] Lo P H, Ashok Kumar S, Chen S M. *Colloids Surf. B*, **2008**, **66**:266-273
- [44] Xie Z, Liu X X, Wang W P, Liu C, Li Z C, Zhang Z J. *Nanoscale Res. Lett.*, **2014**, **9**:105-109
- [45] Qin X Y, Lu W B, Luo Y L, Chang G H, Asiri A M, Al-Youbi A O, Sun X P. *Electrochim. Acta*, **2012**, **74**:275-279
- [46] Yan P, Zhong L, Wen F X, Tang A D. *J. Electroanal. Chem.*, **2018**, **827**:1-9
- [47] Wen X, Long M, Tang A D. *J. Electroanal. Chem.*, **2017**, **785**:33-39
- [48] Alal O, Caglar A, Kivrak H, Sahin O. *Electroanalysis*, **2019**, **31**(9):1646-1655
- [49] Cai L L, Hou B J, Shang Y Y, Xu L, Zhou B, Jiang X N, Jiang X Q. *Chem. Phys. Lett.*, **2019**, **736**:136797
- [50] Chen Q G, Lin T R, Huang J L, Chen Y, Guo L Q, Fu F F. *Anal. Methods*, **2018**, **10**(5):504-507
- [51] Zhang Y T, Deng D M, Zhu X L, Liu S, Zhu Y, Han L, Luo L Q. *Anal. Chim. Acta*, **2018**, **1042**:20-28
- [52] Cheng D, Wang T, Zhang G X, Wu H M, Mei H. *J. Alloys Compd.*, **2020**, **819**:153014
- [53] Chen X R, Gao J, Zhao G Q, Wu C. *Sens. Actuators B*, **2020**, **313**:128038
- [54] Dang W J, Sun Y M, Jiao H, Xu L, Lin M. *J. Electroanal. Chem.*, **2020**, **856**:113592
- [55] Xie F Y, Cao X Q, Qu F L, Asiri A M, Sun X P. *Sens. Actuators B*, **2018**, **255**:1254-1261
- [56] Tian L L, Xia K D, Hu W P, Zhong X H, Chen Y L, Yang C, He G G, Su Y Y, Li L. *Electrochim. Acta*, **2017**, **231**:190-199
- [57] Uzunoglu A, Ipekci H H. *J. Electroanal. Chem.*, **2019**, **848**:113302
- [58] Derbali M, Othmani A, Kouass S, Touati F, Dhaouadi H. *Mater. Res. Bull.*, **2020**, **125**:110771